DOI: 10.21062/mft.2023.108 http://www.journalmt.com

Comparative Evaluation of Working Accuracy in the Atomic Diffusion Additive Manufacturing (ADAM) Process and the Binder Jetting (BJ) Process by Analying Key Characteristics

Andrej Czan (0000-0002-8826-1832)[1], Tatiana Czanova (0000-0002-6943-6393)[1], Jozef Holubjak (0000-0003-3226-9445)[1], Martin Novak (0000-0002-2010-4398)[2], Natalia Czanova (0009-0005-3047-130X)[1], Andrej Czan (0009-0003-9588-4530)[1], Dominik Krisak (0009-0005-3742-272X)[1]
[1]Department of Machining and Production Engineering, Faculty of Mechanical Engineering - University of Žilina, Univerzitna8215/1, 010 26, Žilina, Slovakia. E-mail: andrej.czanstroj.uniza.sk
[2]Faculty of Mechanical Engineering, Jan Evangelista Purkyne University in Usti nad Labem, Pasteurova 3334/7, 400 01 Usti nad Labem. Czech Republic.

This research focuses on comparing the working accuracy of two additive manufacturing processes, Atomic Diffusion Additive Manufacturing (ADAM) and Binder Jetting (BJ). Through the analysis of key characteristics of these processes, we aim to evaluate which one yields better results in terms of working accuracy. ADAM is a process that involves the gradual deposition of metallic materials using a plastic binder, whereas BJ is a process where the binder is applied to powder material, followed by the removal of excess binder. This work conducts a detailed examination of the properties of the ADAM and BJ processes, with a focus on surface texture and microstructure of the resulting objects, the use of optimal technological parameters, and the assessment of dimensional and shape accuracy. It is also important to note that the final nature of 3D objects depends on technological parameters such as geometry, orientation, and placement of individual shape specifications. The results of this study are crucial for assessing the accuracy of these additive processes and can serve as a significant basis for selecting an optimal approach in the field of additive manufacturing.

Keywords: Additive Manufacturing, Metal 3D Objects, Dimensional Accuracy; Shape Accuracy, Surface Roughness

1 Introduction

Additive manufacturing (AM) processes have brought about a transformative shift in how engineers and designers approach product conception and production, primarily due to the increased flexibility in design. Since the advent of rapid prototyping (RP) systems towards the end of the previous century, additive manufacturing machines have made significant advancements, evolving into efficient systems for mass-producing customized products [1]. The absence of the need for specialized tools or molds reduces the economic cost per unit, making additive manufacturing particularly attractive. In the realm of metallic components, there has been a burgeoning interest in this technology due to its ability to create nearly fully dense parts with intricate structures using high-quality materials [2,3]. The principal advantage of additive manufacturing, when compared to traditional subtractive or formative methods, is its demonstrated ability to achieve superior product functionality by effectively harnessing design freedom [4].

Initially, additive manufacturing processes for metallic components were primarily based on powder bed technology, where energy was used selectively to melt the material [1]. Due to the limitations of energy sources in terms of efficiency and power output, these early metallic additive machines were considered indirect production systems, as additional post-processing was required to attain parts with acceptable mechanical performance. In these initial processes, metallic powder was mixed with a polymer binder [5]. A laser beam was used to melt the binder, which acted as a binding agent for metallic particles. The combined material, consisting of both binder and metallic elements, was referred to as the "green part," and additional heat treatment was necessary to remove the binder. To address residual porosity, which could be as high as 40%, the green part was often infiltrated with copper or bronze [6,7]. Examples of these indirect additive manufacturing processes include 3D printing and selective laser sintering (SLS). Subsequently, EOS introduced the direct metal laser sintering (DMLS) system, which eliminated the need for polymer binders as the laser power was sufficient to directly sinter low-melting alloys. In this case, residual porosity was reduced to around 20% [6]. Recent advancements in higher-power energy sources have enabled engineers to overcome these initial

limitations, enabling the production of a broader range of metals directly through additive manufacturing to obtain fully dense (over 99.9%) parts. In some instances, additively manufactured parts exhibit mechanical properties that surpass their cast counterparts. Moreover, controlled build chambers have made it easier to process materials with high melting points and/or oxygen affinity, such as titanium alloys, through additive manufacturing compared to conventional methods [8].

However, powder-based additive processes come with design constraints related to the feasibility of enclosed cavities. After construction, unprocessed powder around the part must be removed through mechanical or manual operations, rendering enclosed cavities inaccessible from the outside. This limitation restricts the design of lightweight parts that might include enclosed lattice structures aimed at providing stiffness without adding significant weight under load. The use of powders also presents challenges when applying powder bed processes in extreme manufacturing environments, such as zero-gravity settings [9], where managing loose powder is impractical. In response to these limitations, additive manufacturing processes based on extrusion have recently emerged and entered the market. These processes draw inspiration from wire welding and fused deposition modeling (FDM) techniques, which have long been employed in layer-by-layer production of polymer and composite parts. Compared to other additive manufacturing processes, extrusion-based methods are more user-friendly and cost-effective, and they can accommodate multi-material deposition.

One such process is Electron Beam Additive Manufacturing (EBAM), which is a direct additive manufacturing method for large-scale metallic components. It involves extruding a metallic wire while simultaneously melting it with an electron beam [8]. Its applications range from rapid prototyping to the production of parts and component repairs. American companies Desktop Metal Inc. and Markforged Inc. [10,11] have recently introduced two new machines that combine fused deposition modeling (FDM) for polymers and metal injection molding (MIM) for metals [12]. MIM is a traditional process used to obtain near-net-shape metallic parts with high complexity [13]. Desktop Metal's patented process is known as Bound Metal DepositionTM (BMD), while Markforged Inc. has named their process Atomic Diffusion Additive Manufacturing (ADAM). Both processes employ a filament comprising metallic powders encapsulated in a thermoplastic polymer, which acts as a binder for the metal particles [14]. This mixture, comprising metal powder particles and polymer, is stored in a cartridge on the machine and is introduced during the process, where the thermoplastic is softened for easy extrusion. BMD uses an ultrasonic vibrator to provide the energy required for bonding the extruded material with the previously deposited material [14], while Markforged Inc. employs a heated extruder [11]. The softened material accumulates and is then pushed through a nozzle or extruder by a piston, layer by layer, onto the build platform [14]. Similar to the MIM process, the as-built part, also referred to as the "green part," is washed to remove the binder (debinding or leaching operation) and then sintered in a furnace to achieve material densification (sintering). Figure 1 illustrates the schematic workflow of the ADAM process. In Markforged Inc.'s system, the binder is thermally debound in a washing system before the sintering phase [15], whereas in Desktop Metal's system, the binder is first removed using a solvent and then subjected to thermal treatment [15]. Due to the presence of the binder and the sintering phase, the part must be oversized and dimensionally adjusted to account for shrinkage during subsequent processing.

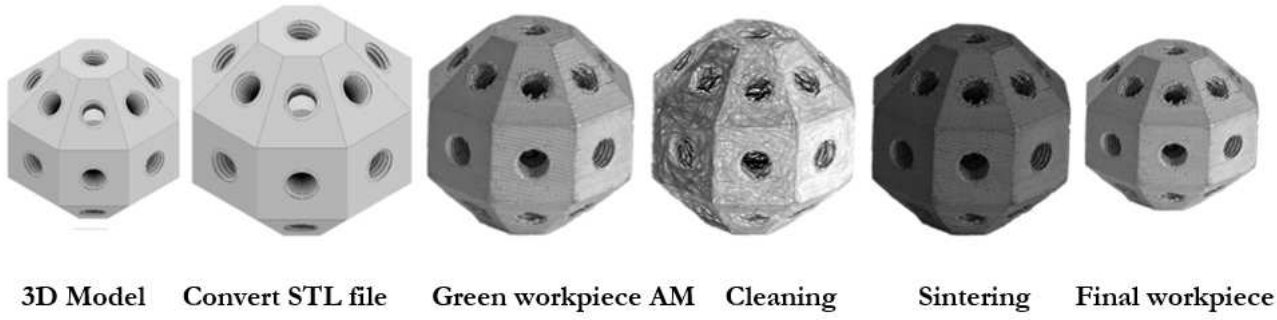

Fig. 1 *Atomic Diffusion Additive Manufacturing (ADAM) workflow*

The objective of this study is to provide essential insights into the working precision of the ADAM process using the Markforged Metal X technological equipment, known for its capabilities in creating complex models leading to the final product. The analysis of working accuracy considers the use of the available 17-4 PH material, which Markforged has developed for industrial applications. The examination of working accuracy focuses on final samples featuring diverse object topologies.

Dimensional and shape accuracy, as well as surface roughness, are assessed across various sample areas. The evaluation of the working accuracy of the ADAM process is defined using IT ISO grades with reference to existing literature.

2 Materials and methods

2.1 Material and equipment for the process ADAM

In 2017, Markforged Inc. introduced its own Metal X technology, designed for the additive manufacturing of metal components (AM). The chemical composition of the Markforged 17-4 PH material is detailed in Table 1 [16]. Markforged 17-4 PH is known for its high strength, hardness, and exceptional corrosion resistance properties. This material finds applications in various industries, including the production of components for oil field valves, chemical processing equipment, aircraft structural components, fasteners, pump shafts, nuclear reactor parts, gears, paper mill machinery, rocket equipment, jet engine components, and more. It's worth noting that 17-4 PH material is a registered trademark of AK Steel.

Tab. 1 *Real values of chemical composition in wt% of material 17-4PH*

Cr	Ni	Cu	Si	Mn	Nb	C	P	S	Fe
16.23	4.2	3.8	0.94	0.87	0.38	0.032	0.026	0.015	Bal

The construction area of the technological equipment measures 300 × 220 × 180 mm, providing a total volume of 11880 cm^3. However, the maximum size of the part that can be manufactured is 250 × 183 × 150 mm. Prior to each operation, a vacuum-sealed sheet is placed on the construction platform to enhance part adhesion during printing and facilitate separation once the process is complete. The base plate and leveling system are engineered to withstand a maximum load of up to 10 kg. The internal space of the device and the baseplate are maintained at specified temperatures throughout the process.

The cleaning procedure is executed within a washing system with a capacity of 18356 cm^3, utilizing a swirling bath containing the cleaning liquid Opteon Sion. The sintering process itself is conducted within a Sinter-2 vacuum furnace with a volume of 18356 cm^3. This furnace can reach temperatures of up to 1300^{o}C and operate in an inert atmosphere using argon and nitrogen. The chamber boasts a cylindrical volume with a diameter of 248 mm and a length of 406 mm.

The size of the part and all parameters of the ADAM process, including the support structures, are automatically generated by proprietary software known as Eiger. Eiger functions as CAM software that manages the entire process from design through to the sintering stage. The software is closed to user modification of process parameters, except for the layer thickness, which determines the machine's resolution. The layer thickness can be adjusted within the range of 0.085 mm to 0.175 mm, with an experimental sample set at a layer height of 0.100 mm. After configuring the layer thickness, the Eiger software calculates volume adjustments to account for part shrinkage during post-printing processes. It then defines the final geometry and shape for printing, along with the polymer infusion time (cleaning time). Additionally, Eiger software outlines the heat treatment procedure for the subsequent sintering step [17,19,20].

2.2 Material and equipment for the BJ process

Binder Jetting technology operates by depositing a liquid binding agent selectively onto a layer of powdered material, typically metal, to create parts. It builds the desired shape layer by layer. This technology starts with a platform that is evenly coated with a layer of metallic powder. A liquid binding agent is then precisely applied to the chosen areas using a controlled process. The binding agent solidifies the powder, creating the first layer of a 3D object. Once the process is finished, the solidified part needs to be cleaned to remove any leftover loose powder particles.

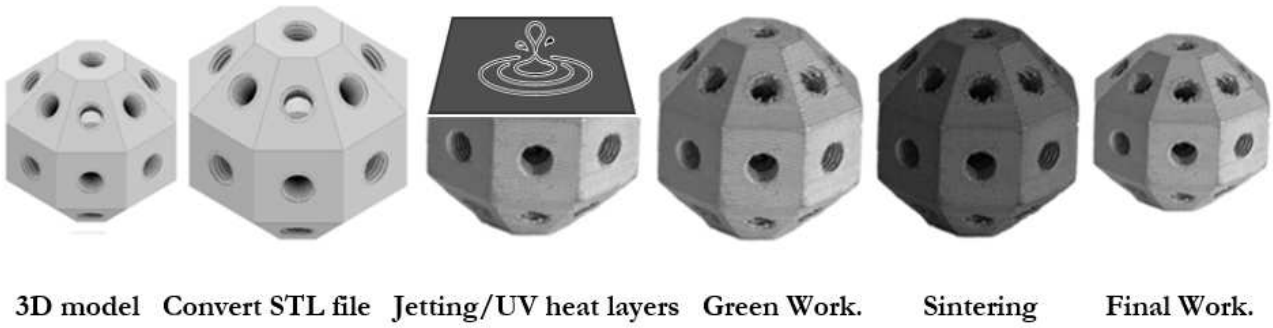

Fig. 2 *Binder Jetting (BJ) workflow*

The material used for creating experimental samples was identical to the one used in the ADAM 17-4PH process. The chemical composition of the material adhered to the standard's specified mass fractions. Following the layering process, the samples underwent sandblasting to eliminate any excess metal powder.

2.3 Design of experimental samples

The design of the experimental sample is based on the creation of reference areas aligned with the X, Y, and Z coordinate system orientations. As we are aware, additive manufacturing technologies result in diverse layer formation and properties after solidification, which are heavily influenced by the sample's orientation within the X, Y, and Z axes of the build chamber and the direction of layer application. While there exists a substantial number of reference samples for comparative analysis and detailed object creation in AM technologies, these samples often fail to account for the impact of specific orientations and layering directions of 3D models.

To facilitate a comprehensive volumetric analysis in three-dimensional orientations, it is advisable to design the sample to encompass all possible orientations, including areas with both positive and negative angles along the Z-axis. Consequently, the sample was crafted with a three-dimensional orientation in mind, creating octagonal-shaped regions where all faces of the model maintain equal distances and are parallel to each other, as depicted in Figure 3. These parallel faces are separated by a distance of 30 mm, holes within the samples possess a diameter of 5 mm, and threaded samples feature an M6 thread.

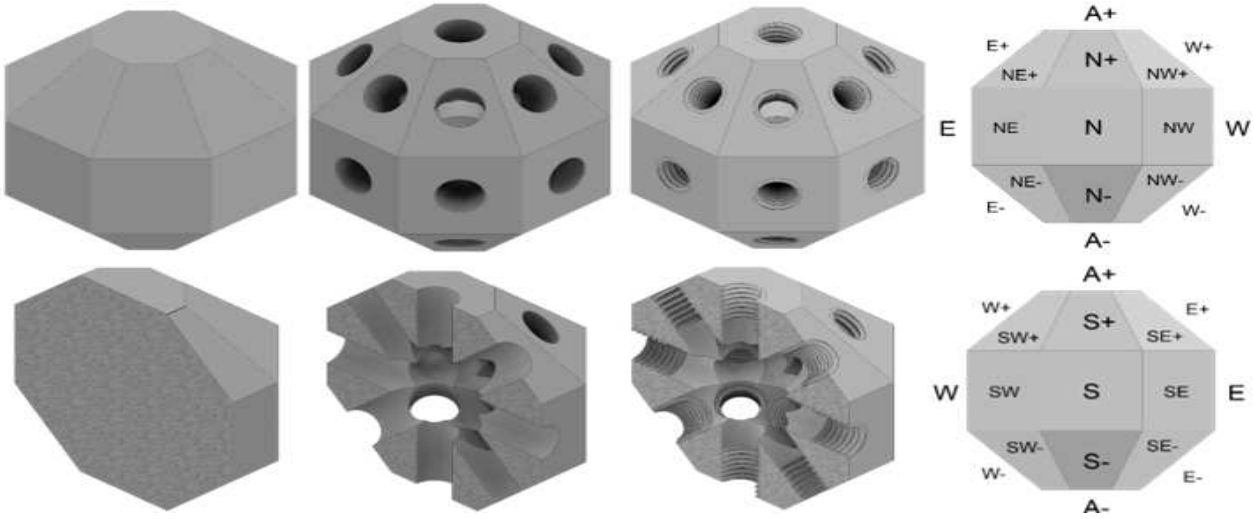

Fig. 3 *View 3D models of samples in full shape (P) with holes (D) and threads (Z) and view of the detail of the samples in the section, where the NSEW+/-A system of marking the monitored areas is shown on the right*

The sample design comprises eight square areas positioned in the XY plane. Within the Z orientation, there are two parallel octagonal faces, categorized as surfaces with positive and negative inclinations. As a result of the surfaces connecting square and octagonal facets, trapezoidal surfaces emerge, with slopes either in a positive or negative orientation. Altogether, the proposed sample features 26 surfaces that run parallel to each other, effectively creating a 26-sided spherical object of the Revolved Sphere category. These designed samples facilitate the assessment of working accuracy, allowing for the analysis of dimensional and shape specifications as well as surface roughness.

3 Evaluation of experimental trials

3.1 Evaluation of real samples and surface texture

Following the design, physical samples were manufactured in their complete form, featuring holes and threads created directly during the layering process. These samples were oriented based on the Cartesian coordinate system outlined in Figure 3. To simplify the spatial orientation designation, we utilized the X-axis as the East-West axis (E-W), the Y-axis as the North-South axis (N-S), and the Z-axis as A+ and A-.

The samples exhibit eight square faces in the XY orientation, designated as per the directions NSEW+/-A and their 45° combinations, namely NE, NW, SE, and SW. In the Z orientation, two parallel octagonal faces were labeled as faces A with positive (+) and negative (-) inclinations. This system was implemented to subsequently identify the distinct regions of a spherical object. Based on the applied markings, samples were then produced at various bases within the technological equipment. Figure 4 illustrates objects created through the ADAM technology process, while Figure 5 showcases samples produced using the BJ technology process.

Fig. 4 *Depicts the realistic identification of experimental samples created using ADAM technology, showcasing three different variants: plan P, with holes D, and threaded Z*

Fig. 5 *Depicts the realistic identification of experimental samples created using BJ technology, showcasing three different variants: plan P, with holes D, and threaded Z*

To characterize the generated surfaces and their fundamental parameters, including directness (P), roughness (R), and corrugation (W), we utilized the Infinite Focus G5 device. The Infinite Focus G5 combines optical micro-coordinate measurement and surface roughness measurement within a single system. It is a highly precise, rapid, and versatile optical 3D measurement system. The integration of a 3D micro-coordinate measuring machine and a surface roughness measurement device results in a comprehensive two-in-one system. The system's capacity to measure surfaces is nearly limitless, making it suitable for assessing the relative surface properties of micro-precision components using a single multifunctional measurement sensor. This technology enables exceptionally precise and consistent measurements with vertical resolutions as fine as 10nm [17,19,22]. Employing hardware-assisted vibration dampening and focusing variation, this measurement method can evaluate the shape and surface roughness of large and heavy objects[20]. The Infinite Focus is equipped with built-in high-precision positioning devices on its axes, ensuring accurate movement in the X and Y planes[18,21,23]. Furthermore, its automated interface allows for fully automatic measurements in production settings. Figure 6 illustrates the analyzed scanned areas in position 'S.'

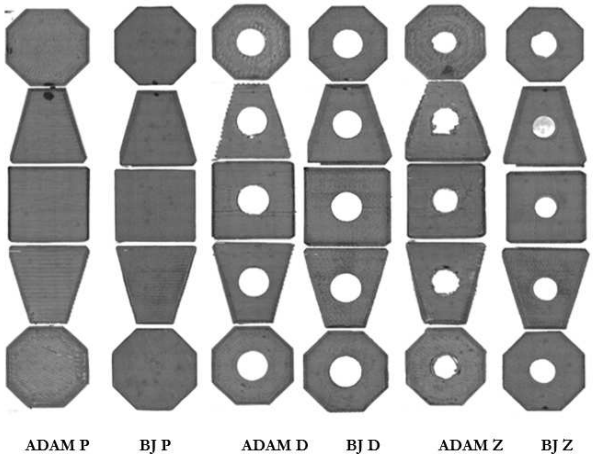

Fig. 6 *Displays images of scanned surfaces in the "S" position for experimental samples in three variations: solid P, with holes D, and threaded Z*

3.2 Evaluation of surface parameters P, R and W

We primarily examined the arithmetic mean deviation of the profile, denoted as Pa, Ra, and Wa in our case. It is calculated as the arithmetic average of the absolute deviations of the profile Z(x) within their respective base lengths [22,24,29].

$$Pa, Ra, Wa = \frac{1}{l}\int_0^l /Z(x)/dx \ , \ for \ \mathrm{l} = \mathrm{lp, lr \ or \ lw} \quad [\mathrm{mm}] \tag{1}$$

The mean quadratic deviation of the profiles under consideration, denoted as Pq, Rq, and Wq in our case, is calculated as the mean quadratic value of the absolute deviations of the profile Z(x) within their respective base lengths [22,24,29].

$$Pq, Rq, Wq = \sqrt{\frac{1}{l}\int_0^l Z(x)^2 \, dx} \ , \ \text{for } \mathrm{l} = \mathrm{lp, lr \ or \ lw} \quad [\mathrm{mm}] \tag{2}$$

The total height, represented as Pz, Rz, and Wz, is calculated by adding the maximum peak height (Zp) and the maximum depression depth (Zv) of the profile within the evaluation length, not the sampling length. The relationship Rt≧Rz holds true for all profiles. Additionally, Pt signifies the maximum total section height, and Wt represents the maximum total corrugation height [22,24,29].

$$Pz, Rz, Wz = maxZp + maxZv \ , \ \text{for } \mathrm{l} = \mathrm{lp, lr \ or \ lw} \quad [\mathrm{mm}] \tag{3}$$

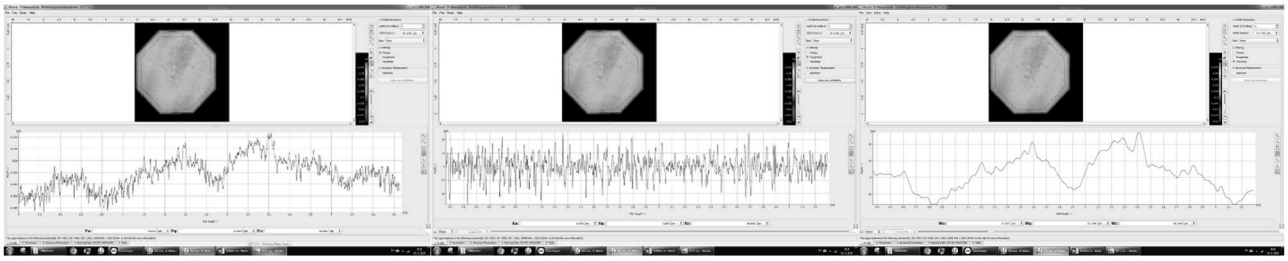

Fig. 7 *Model of examined surfaces for the complete sample and area A+, with the parameters Ra, Rq, and Rz determined*

The technology device was configured to analyze samples produced using both BJ and ADAM technologies, focusing on full samples (P), hole models (D), and threaded models (Z). Each of these samples was subjected to surface scanning in orientations denoted as A+, S+, S, S-, and A-. A representation of the scanning results is illustrated in Figure 7. Subsequently, we evaluate various parameters, including Pa, Ra, Wa, Pq, Rq, Wq, Pz, Rz, and Wz. The comparison encompasses scanned surfaces for all three types of experimental samples, with the surface analysis presented in the color map depicted in Figure 8.

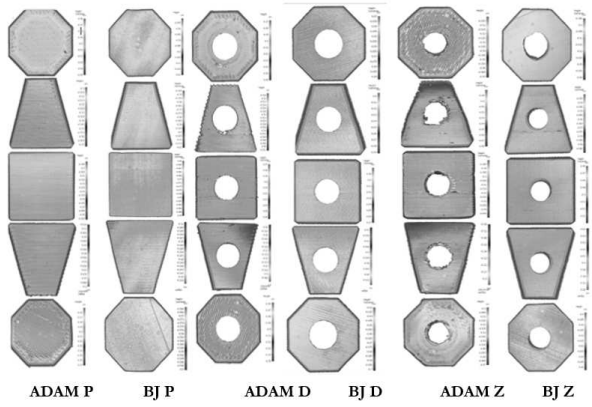

Fig. 8 *Images of scanning surfaces in the "S" position, featuring texture identification through a color map, for experimental samples denoted as solid P, those with holes D, and those with Z threads*

3.3 Methodology for Evaluating Working Accuracy

The objective of the working accuracy analysis is to assess the dimensional and shape precision achievable through both the BJ process and ADAM process. This analysis was conducted using reference samples specifically designed to ascertain the fundamental precision characteristics of AM processes(25). These reference parts feature straightforward geometries of varying dimensions that gauge the accuracy across the initial eight basic size ranges, with their faces being parallel to one another (as illustrated in Figure 3). Dimensional and geometric tolerances, encompassing shape imperfections, are scrutinized for both convex and concave aspects of the artifact, following a specific system.

The evaluation of dimensional accuracy for the replica adhered to ISO 286-1:1988(26) standards. Within each ISO base size range, the dimensional accuracy for both the BJ process and ADAM process was assessed in relation to the achieved IT level of the replica artifact. In particular, the IT precision level was established under the assumption that the maximum dimensional error corresponds to the number of unit tolerances (n) corresponding to the 95th percentile of the distribution of the number of unit tolerances (nj) for each general jth dimension. The calculation of nj is as follows:

$$n_j = \frac{1000|D_{jn} - D_{jm}|}{i} \tag{4}$$

In the provided formula, Djn represents the nominal dimension, Djm signifies the actual dimension of the characteristic, and i represents a tolerance factor that varies across different ranges of the basic ISO sizes, as outlined in Table 2. The actual dimension is calculated as the average of three measurements of a geometric feature of the replica. These measurements were conducted using the Zeiss Eclipse coordinate measuring machine (CMM), with the CMM model being GLOBAL Image 07.07.07. This model has a specified maximum permissible error (MPEE) of 2.2 μm + L/1000 in accordance with ISO-10360/2 [27], where L represents the measured length. Table 3 provides the classification of dimensional quality, as ISO IT grades are contingent upon the value of n [28,29].

Tab. 2 *International Organisation for Standardisation (ISO) basic size ranges and corresponding tolerance factor i*

Range	Basic Size							
Above D_1 (mm)	1	3	6	10	18	30	50	80
Up to including D_2 (mm)	3	6	10	18	30	50	80	120
Standard tolerance factor *i* (μm)	0.542	0.733	0.898	1.083	1.307	1.561	1.856	2.173

Tab. 3 *Classification of IT levels according to ISO 286-1:1988*

Range		IT 10	IT 11	IT 12	IT 13	IT 14	IT 15	IT 16
Above 1 mm	Up to 500 mm	64i	100i	160i	250i	400i	640i	1000i

4 Results and discussion

Following the scanning of individual surfaces using the InfiniteFocus G5 optical measuring device, we conducted comprehensive comparisons of the surface parameters that were attained. These comparisons were based on the results obtained, enabling us to evaluate the impact of technology and surface shape on the outcomes across various orientations (A+, S+, S, S-, A-) for the solid P model with holes D and threaded Z model, each produced by a distinct technology. Subsequently, we compared the results concerning surface properties between the different technologies. Figures 9 to 11 provide a summary of the measured deviations, their average values, as well as the standard deviation, visually presented in a polar display.

Upon reviewing the graphs, it becomes evident that the sample created using the Binder Jetting technology exhibited the most favorable values among the examined samples. Meanwhile, the sample produced via ADAM technology demonstrated superior outcomes for the Full Sample.

Pa		ADAM	BJ	Ra		ADAM	BJ	Wa		ADAM	BJ
A+		14,82	18,83	A+		4,78	17,20	A+		13,63	17,20
S+		36,58	38,84	S+		15,46	32,23	S+		31,41	32,23
S		42,73	20,04	S		6,78	17,21	S		17,52	17,21
S-		25,42	31,66	S-		11,90	29,06	S-		19,43	29,06
A-		93,96	20,83	A-		14,31	19,55	A-		83,08	19,55
Average		42,70	26,04	Average		10,64	23,05	Average		33,01	23,05
St. deviat.		30,58	8,81	St. deviat.		4,68	7,09	St. deviat.		28,76	7,09

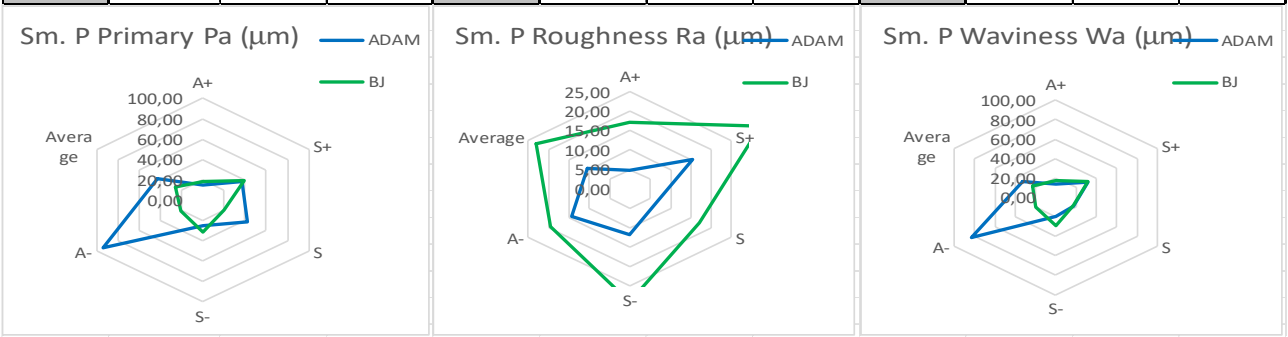

Fig. 9 *Assessment of measured values pertaining to straightness, roughness, and corrugation of the profile (Pa, Ra, Wa) and their comparison presented in a polar graph for the P sample produced using both ADAM and BJ technologies*

Pa		ADAM	BJ	Ra		ADAM	BJ	Wa		ADAM	BJ
A+		74,34	20,26	A+		40,63	17,06	A+		43,39	17,06
S+		27,47	34,49	S+		9,34	28,03	S+		24,68	28,03
S		15,81	12,98	S		5,88	10,22	S		13,32	10,22
S-		89,77	38,22	S-		12,06	34,93	S-		74,99	34,93
A-		25,07	20,91	A-		5,16	18,56	A-		19,40	18,56
Average		46,49	25,37	Average		14,61	21,76	Average		35,16	21,76
St. deviat.		33,21	10,58	St. deviat.		14,80	9,72	St. deviat.		24,95	9,72

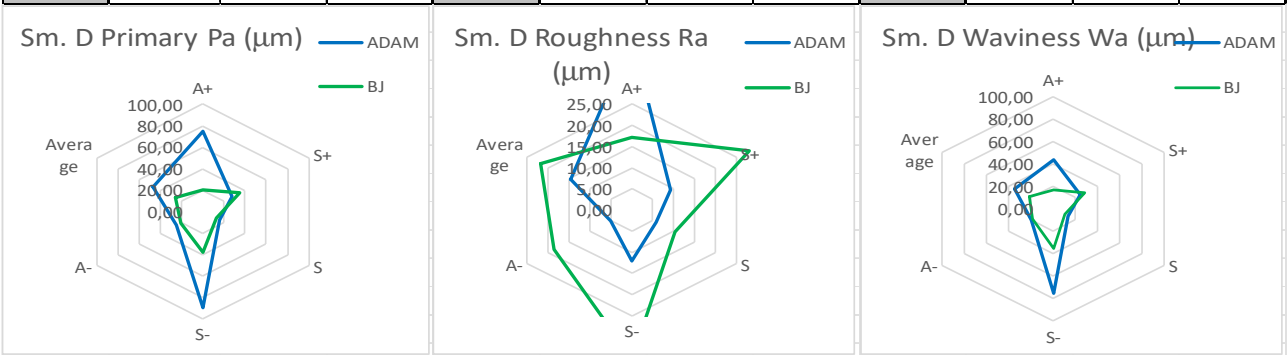

Fig. 10 *Assessment of measured values pertaining to straightness, roughness, and corrugation of the profile (Pa, Ra, Wa) and their comparison presented in a polar graph for the D sample produced using both ADAM and BJ technologies*

Pa		ADAM	BJ	Ra		ADAM	BJ	Wa		ADAM	BJ
A+		53,22	28,30	A+		4,94	25,81	A+		52,60	25,81
S+		125,89	37,06	S+		11,01	32,44	S+		120,14	32,44
S		13,65	21,68	S		6,49	18,91	S		10,14	18,91
S-		122,43	14,96	S-		9,87	11,18	S-		116,18	11,18
A-		49,69	19,92	A-		25,39	17,77	A-		36,21	17,77
Average		72,98	24,39	Average		11,54	21,22	Average		67,06	21,22
St. deviat.		49,24	8,54	St. deviat.		8,12	8,14	St. deviat.		49,07	8,14

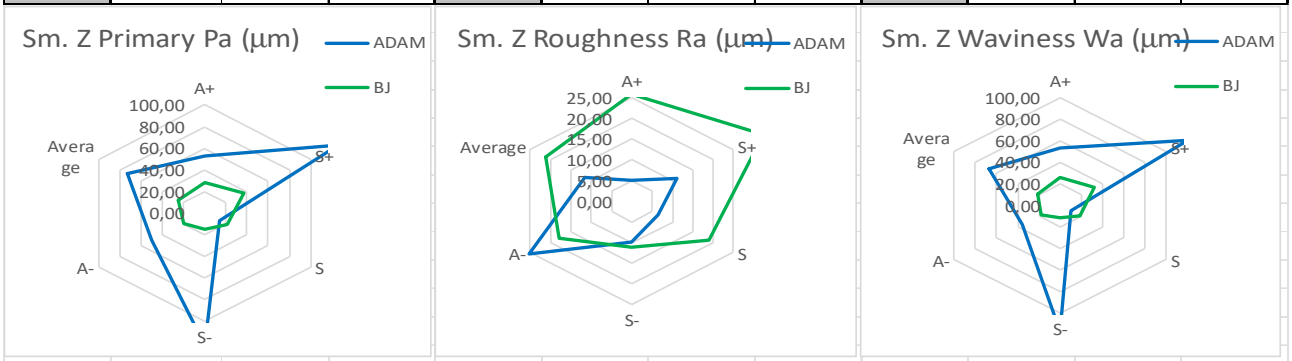

Fig. 11 *Assessment of measured values pertaining to straightness, roughness, and corrugation of the profile (Pa, Ra, Wa) and their comparison presented in a polar graph for the Z sample produced using both ADAM and BJ technologies*

The samples were measured using the Alicona InfiniteFocus G5 device, with a 5x magnification objective. The graphs in Figures 9 to 11 depict the individual examined samples produced by different AM technologies, comparing their primary surface parameters Pa, roughness Ra, and waviness Wa. The best roughness values were achieved by the solid samples, with ADAM technology yielding the most favorable results. In the case of the BJ process, significantly better values were obtained for the primary profile and waviness of the experimental samples, particularly for samples with holes. When comparing the two technologies, ADAM exhibits excellent characteristics in terms of surface roughness, while BJ technology shows significantly better parameters in terms of primary profile and surface waviness. The primary profile and waviness are directly related to the dimensional accuracy of 3D objects.

The collected data were subsequently processed to assess the precision of the applied AM technologies, specifically ADAM and BJ. We examined the upper and lower dimension limits with a predefined tolerance of ±0.2mm, analyzing the deviations from this tolerance. We then evaluated the technology's accuracy by determining the standard tolerance factor "i," calculating average measured values, and assessing the deviations from the nominal dimensions. Subsequently, we established tolerance ranges and determined the IT accuracy levels.

The IT accuracy levels were examined for all measured values of individual surfaces, comparing the minimum, average, and maximum tolerance ranges. The results were visualized using polar graphs, both for the employed AM technologies and their 3D models of different shapes, namely P, D, and Z, Figs. 12 to 17.

AREA	IT range min. [mm]	IT range avg. [mm]	IT range max. [mm]	ITx min	ITx average	ITx max
A1/A2	96	180	230	IT11	IT12	IT13
N/S	21	1	13	IT8	IT0-4	IT7
NW/SE	6	4	12	IT5	IT0-4	IT6
W/E	83	72	62	IT11	IT10	IT10
SW/NE	101	87	66	IT11	IT11	IT10
N+/S-	126	117	106	IT11	IT11	IT11
N-/S+	97	76	38	IT11	IT10	IT9
NW+/SE-	102	85	65	IT11	IT11	IT10
NW-/SE+	97	79	61	IT11	IT10	IT10
W+/E-	119	90	28	IT11	IT11	IT8
W-/E+	136	114	81	IT12	IT11	IT10
SW+/NE-	111	95	67	IT11	IT11	IT10
SW-/NE+	152	133	89	IT12	IT12	IT11
Average	96	87	71	IT11	IT11	IT10
min	6	1	12	IT5	IT0-4	IT6
max	152	133	106	IT12	IT12	IT11

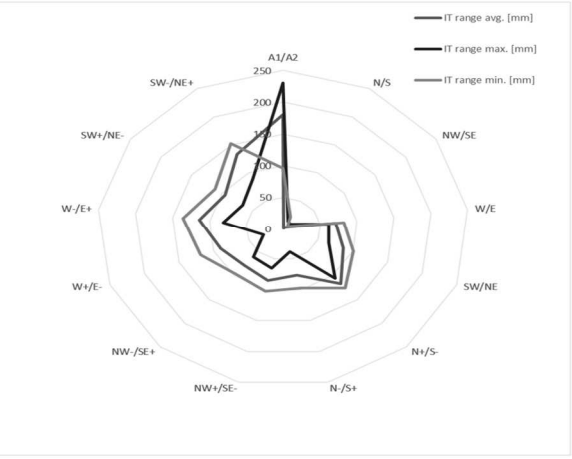

Fig. 12 *Measured data obtained for ADAM technology, sample shape "full P," and their visual representation in a polar view for comparison*

AREA	IT range min. [mm]	IT range avg. [mm]	IT range max. [mm]	ITx min	ITx average	ITx max
A1/A2	69	171	272	IT10	IT12	IT13
N/S	15	62	109	IT7	IT10	IT11
NW/SE	36	52	116	IT9	IT10	IT11
W/E	61	4	65	IT10	IT0-4	IT10
SW/NE	0	7	20	IT0-4	IT5	IT7
N+/S-	115	78	50	IT11	IT10	IT9
N-/S+	139	99	31	IT12	IT11	IT8
NW+/SE-	48	36	27	IT9	IT9	IT8
NW-/SE+	140	79	0	IT12	IT10	IT0-4
W+/E-	109	69	23	IT11	IT10	IT8
W-/E+	193	139	76	IT12	IT12	IT10
SW+/NE-	113	97	58	IT11	IT11	IT10
SW-/NE+	156	144	130	IT12	IT12	IT11
Average	92	80	75	IT11	IT10	IT10
min	0	4	0	IT0-4	IT0-4	IT0-4
max	193	144	130	IT12	IT12	IT11

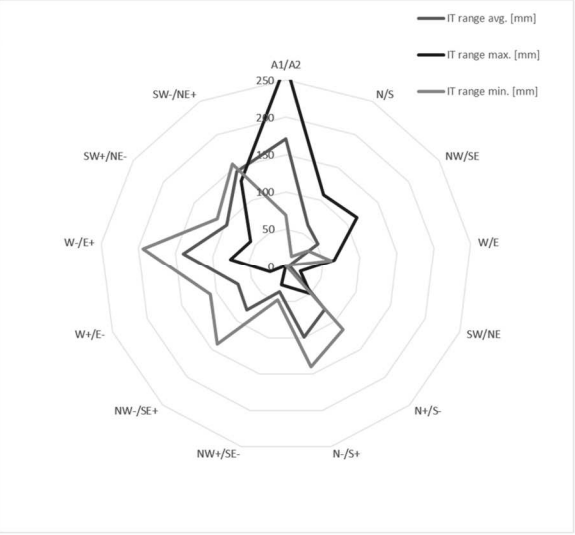

Fig. 13 *Measured data obtained for ADAM technology, sample shape "hole D," and their visual representation in a polar view for comparison*

AREA	IT range min. [mm]	IT range avg. [mm]	IT range max. [mm]	ITx min	ITx average	ITx max
A1/A2	106	55	31	IT11	IT10	IT8
N/S	15	1	34	IT7	IT0-4	IT9
NW/SE	8	21	41	IT5	IT8	IT9
W/E	67	32	5	IT10	IT8	IT0-4
SW/NE	84	62	35	IT11	IT10	IT9
N+/S-	88	47	11	IT11	IT9	IT6
N-/S+	196	57	55	IT12	IT10	IT10
NW+/SE-	132	43	43	IT12	IT9	IT9
NW-/SE+	140	100	71	IT12	IT11	IT10
W+/E-	161	77	17	IT12	IT10	IT7
W-/E+	152	109	31	IT12	IT11	IT8
SW+/NE-	202	60	27	IT12	IT10	IT8
SW-/NE+	220	73	45	IT13	IT10	IT9
Average	121	57	34	IT11	IT10	IT9
min	8	1	5	IT5	IT0-4	IT0-4
max	220	109	71	IT13	IT11	IT10

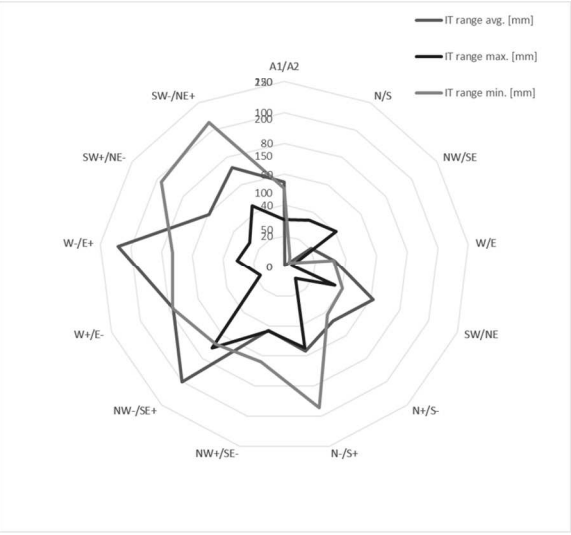

Fig. 14 *Measured data obtained for ADAM technology, sample shape "thread Z," and their visual representation in a polar view for comparison*

AREA	IT range min. [mm]	IT range avg. [mm]	IT range max. [mm]	ITx min	ITx average	ITx max
A1/A2	526	517	508	IT15	IT15	IT15
N/S	214	245	281	IT13	IT13	IT13
NW/SE	147	163	175	IT12	IT12	IT12
W/E	172	183	190	IT12	IT12	IT12
SW/NE	300	330	368	IT13	IT14	IT14
N+/S-	237	222	214	IT13	IT13	IT13
N-/S+	341	329	311	IT14	IT14	IT13
NW+/SE-	185	177	172	IT12	IT12	IT12
NW-/SE+	476	447	429	IT14	IT14	IT14
W+/E-	170	162	149	IT12	IT12	IT12
W-/E+	457	426	402	IT14	IT14	IT14
SW+/NE-	221	202	193	IT13	IT12	IT12
SW-/NE+	301	272	255	IT13	IT13	IT13
Average	288	283	281	IT13	IT13	IT13
min	147	162	149	IT12	IT12	IT12
max	476	447	429	IT14	IT14	IT14

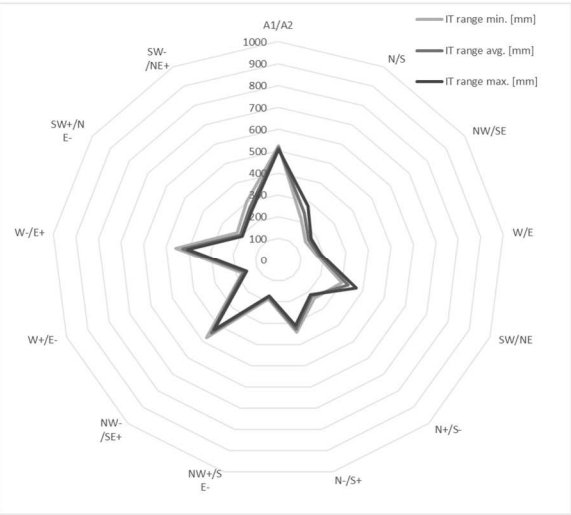

Fig. 15 *Measured data obtained for BJ technology, sample shape "full P," and their visual representation in a polar view for comparison*

AREA	IT range min. [mm]	IT range avg. [mm]	IT range max. [mm]	ITx min	ITx average	ITx max
A1/A2	1022	999	981	IT16	IT16	IT16
N/S	15	24	31	IT7	IT8	IT8
NW/SE	75	91	109	IT10	IT11	IT11
W/E	239	251	262	IT13	IT13	IT13
SW/NE	134	137	142	IT12	IT12	IT12
N+/S-	507	475	450	IT15	IT14	IT14
N-/S+	776	746	705	IT15	IT15	IT15
NW+/SE-	414	411	404	IT14	IT14	IT14
NW-/SE+	784	729	693	IT15	IT15	IT15
W+/E-	455	428	397	IT14	IT14	IT14
W-/E+	616	579	523	IT15	IT15	IT15
SW+/NE-	597	588	574	IT15	IT15	IT15
SW-/NE+	550	529	505	IT15	IT15	IT14
Average	476	461	444	IT14	IT14	IT14
min	15	24	31	IT7	IT8	IT8
max	784	746	705	IT15	IT15	IT15

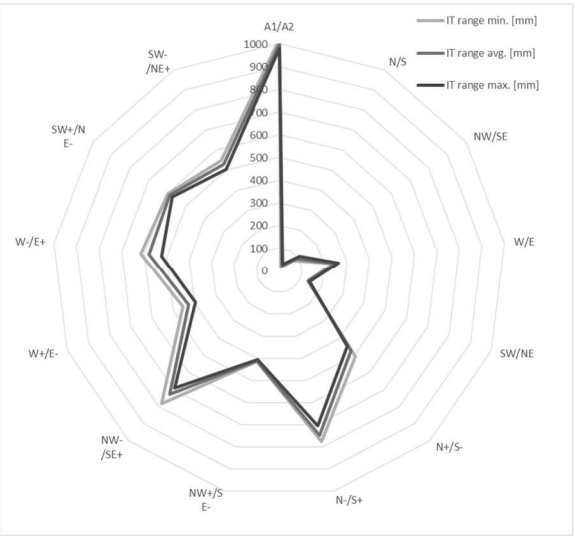

Fig. 16 *Measured data obtained for BJ technology, sample shape "hole D," and their visual representation in a polar view for comparison*

AREA	IT range min. [mm]	IT range avg. [mm]	IT range max. [mm]	ITx min	ITx average	ITx max
A1/A2	731	710	695	IT15	IT15	IT15
N/S	121	143	154	IT11	IT12	IT12
NW/SE	165	217	272	IT12	IT13	IT13
W/E	154	172	190	IT12	IT12	IT12
SW/NE	117	129	140	IT11	IT11	IT12
N+/S-	273	258	249	IT13	IT13	IT13
N-/S+	547	516	469	IT15	IT15	IT14
NW+/SE-	349	330	304	IT14	IT14	IT13
NW-/SE+	438	430	413	IT14	IT14	IT14
W+/E-	475	452	434	IT14	IT14	IT14
W-/E+	368	343	329	IT14	IT14	IT14
SW+/NE-	564	537	511	IT15	IT15	IT15
SW-/NE+	280	263	245	IT13	IT13	IT13
Average	352	346	339	IT14	IT14	IT14
min	117	129	140	IT11	IT11	IT12
max	564	537	511	IT15	IT15	IT15

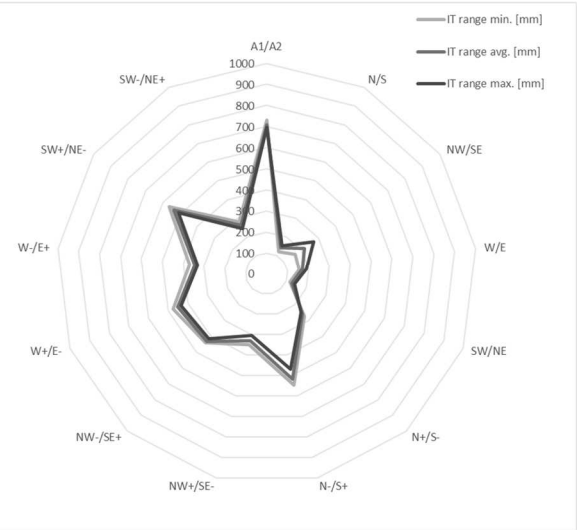

Fig. 17 *Measured data obtained for BJ technology, sample shape "thread Z," and their visual representation in a polar view for comparison*

The comparison was conducted between samples produced using two distinct technologies, with a focus on assessing the IT precision levels of each sample. The samples created through ADAM technology demonstrated an average IT precision level ranging from IT7 to IT11. The most favorable outcomes were observed for the sample featuring holes and threads, while the full sample exhibited slightly lower precision.

In contrast, the Binder Jetting technology yielded less satisfactory results, with precision levels spanning from IT14 to IT15. The full sample displayed the best precision performance among the Binder Jetting samples, while samples with holes and threads demonstrated similar IT precision levels.

In summary, ADAM technology outperformed Binder Jetting, achieving IT precision levels ranging from IT5 to IT11, with the most exceptional results witnessed in the threaded sample. Samples with holes and the full sample exhibited comparable IT precision levels. Surfaces parallel to the Z-axis exhibited significantly higher precision than slanted surfaces, with ADAM technology achieving IT precisions of 0-4 for the latter.

5 Conclusions

The article presents the results of analyses focused on the working accuracy and surface roughness of 3D objects made from 17-4PH material produced using the Atomic Diffusion Additive Manufacturing (ADAM) process patented by Markforged Inc., with subsequent comparison to the Binder Jetting (BJ) process. The aim of the analysis is to enhance our understanding of the ADAM and BJ processes, with a focus on evaluating the fundamental characteristics of working precision, for potential industrial

implementations. Despite the added value and positive aspects of these processes, they are currently underexplored.

The results obtained from these experiments help assess the effectiveness, precision, quality, and reliability of both technologies. The experiments were divided into three parts, analyzing surface texture, surface roughness, and working accuracy. The surface texture experiment evaluated the surfaces of samples created using both technologies, considering their different orientations. The results showed that the ADAM technology performed better in terms of surface roughness, while the BJ technology achieved significantly better results in primary profile parameters and surface waviness, particularly in uniform distribution.

Regarding dimensional precision, all samples underwent comprehensive measurements, and the resulting IT (International Tolerance) precision, at which individual samples were produced, was determined based on the measured results. The sample produced using the ADAM technology exhibited better precision parameters compared to the BJ technology. The ADAM technology achieved IT precision ranging from IT5 to IT11, which is 5 degrees better than the SLM (Selective Laser Melting) technology and more.

In conclusion, the experiments revealed that the ADAM technology is more suitable for manufacturing components with complex geometric shapes. This technology excels in IT precision, surface texture, and minimizes the need for subsequent processing. These results have significance in the field of additive manufacturing of metal components, as they provide a comparison between two advanced technologies in terms of precision, hardness, and surface design. The ADAM process continues to gain success, and its positive characteristics are gradually being implemented into manufacturing processes. These components have lower weight due to their internal lattice-like design, making them suitable for environmental applications. The filament-based ADAM process is evolving as a viable and economically efficient alternative for component manufacturing, with simpler material control compared to powder-based metal additive manufacturing. Future research could focus on studying the impact of various heat treatments on the microstructure, static, and dynamic properties of these components.

Acknowledgement

This research was funded by the University of Žilina project VEGA 1/0520/21 Research of the integrity of surfaces created by the additive process of atomic diffusion of metal-elastomer fibers with post-process of productive machining, next project KEGA 063ŽU-4/2021: "Integration of detection-visualization technologies for innovative additive manufacturing technologies as an online tool for creative and critical thinking".

References

[1] GALATI, M.; MINETOLA, P.; Analysis of Density, Roughness, and Accuracy of the Atomic Diffusion Additive Manufacturing (ADAM) Process for Metal Parts. *Materials 2019*, 12, 4122; doi:10.3390/ma12244122, 1-15

[2] LEE, H.; LIM, C.H.J.; LOW, M.J.; THAM, N.; MURUKESHAN, V.M.; KIM, J.-J. Lasers in additive manufacturing: an overview. *Int. J. Precis. Angl. Manuf. Green technol. 2017*, 4, 307–322

[3] BIAMINO, S.; PENNA, A.; ACKELID, U.; SABBADINI, S.; TASSA, O.; FINO, P.; PAVESE, M.; GENNARO, P.; BADINI, C. Electron beam melting of the alloy Ti–48Al–2Cr–2Nb: Investigation of microstructure and mechanical properties. *Intermetallic Substances 2011*, 19, 776–781

[4] GIBSON, I.; ROSEN, D.W.; STUCKER, B. AM technologies; *Springer: New York*, NY, USA, 2015

[5] SAADLAOUI, Y.; MILAN, J.-L.; ROSSI, J.-M.; CHABRAND, P. Topology optimization and additive manufacturing: Comparison of design methods using industry codes. *J. Manuf. Syst. 2017*, 43, 178–186

[6] KRUTH, J.-P.; LEU, M.-C.; NAKAGAWA, T. Advances in additive manufacturing and rapid prototyping. *CIRP Ann. 1998*, 47, 525–540

[7] MCALEA, K. Materials and applications for selective laser sintering. In *Proceedings of the 7th International Conference on Rapid Prototyping*, San Francisco, CA, USA, March 31-April 3, 1997; pp. 23-33

[8] GALATI, M.; IULIANO, L. Literature review on powder-based electron beam melting with a focus on numerical simulations. *Add. Manuf. 2018*, 19, 1–20

[9] SGAMBATIA, A.; BERGA, M.; ROSSIA, F.; DAURSKIKHB, A.; IMHOFC, B.; DAVENPORTC, R.; WEISS, P.; PEER, M.; GOBERT, T.; MAKAYA, A. URBAN: Lunar base design using 3D printing technologies. In *Proceedings of the 69th International Astronautical Congress*, Bremen, Germany, 1-5 October 2018; pp. 1-9

[10] CAMPBELL, R.I.; WOHLERS, T. MARKFORGED: A different approach to

metal additive manufacturing. Available online: http://www.metal-am.com/wp-content/uploads/sites/4/2017/06/MAGAZINE-Metal-AM- Summer-2017-PDF-sp.pdf (accessed 23 July 2019)

[11] Markforged. Materials. Available online: https://markforged.com/blog/metal-3d-printing-materials/ (accessed 5 December 2019)

[12] SPENCER, O. O.; YUSUF, O. T.; TOFADE, T. C. The evolution of additive manufacturing technology: a trajectory towards the industrial revolution. *Am. J. Moss. Ind. Eng. 2018*, 3, 80–90

[13] BHERO, S. Metal injection molding as a possible processing pathway for porous prostheses. *Int. J. Res. Chem. Metall. Civ. Eng. 2014*, 1, 50–53

[14] WOHLERS, T. DESKTOP METAL: Vychádzajúca hviezda kovovej aditívnej výroby sa zameriava na rýchlosť, náklady a veľkoobjemovú výrobu. Kovová AM. Online: http://www.metal-am.com/wp-content/uploads/sites/4/2017/06/MAGAZINE- Kov-AM-Leto-2017-PDF-sp.pdf (prístup k 23. júlu 2019)

[15] GONZALEZ-GUTIERREZ, J.; CANO, S.; SCHUSCHNIGG, S.; COCOON, C.; SAPKOTA, J.; HOLZER, C. Additive manufacturing of metal and ceramic components by extrusion of highly filled polymer materials: an overview and future perspectives. *Materials 2018*, 11, 840

[16] Markforged. Stainless steel 17-4 PH. Material datasheet. Available online: https://static.markforged.com/download/markforged_datasheet_17-4_ph_stainless_steel.pdf (accessed 5 December 2019)

[17] TIMKO, P.; HOLUBJAK, J.; BECHNÝ, V.; NOVÁK, M.; CZÁN, A.; CZÁNOVÁ, T.; Surface Analysis and Digitization of Components Manufactured by SLM and ADAM Additive Technologies, *Manufacturing Technology 2023*, 23(1):127-134, DOI: 10.21062/mft.2023.008

[18] THIPPRAKMAS, S.; SONTAMINO, A.; PHANITWONG, W.; Finite Element Analysis of Counterbore-shaped Parts by Using Sheet-bulk Metal Forming Process, *Manufacturing Technology 2017*, 17(4):597-602, DOI: 10.21062/ujep/x.2017/a/1213-2489/MT/17/4/597

[19] TIMKO, P.; CZÁNOVÁ, T.; CZÁN, A.; SLABEJOVÁ, S.; HOLUBJAK, J.; CEDZO, M.; Analysis of Parameters of Sintered Metal Components Created by ADAM and SLM Technologies, *Manufacturing Technology 2022*, 22(3):347-355, DOI: 10.21062/mft.2022.032

[20] BURGEROVA, K.; HERMAN, A.; The issue of regeneration of metal powder DLMS 3D printing, *Manufacturing Technology 2020*, 20(1):11-17 | DOI: 10.21062/mft.2020.014

[21] PANNETON, R.; GROŠ, E. Missing mass method for measuring the open porosity of porous solids. *Acta Acust. United Acust. 2005*, 91, 342–348

[22] KOZOVÝ, P.; ŠAJGALÍK, M.; DRBÚL, M.; HOLUBJÁK, J.; MARKOVIČ, J.; JOCH, R.; BALŠIANKA, R.; Identification of Residual Stresses after Machining a Gearwheel Made by Sintering Metal Powder, *Manufacturing Technology 2023*, 23(4):468-474, DOI: 10.21062/mft.2023.054

[23] MESICEK, J.; RICHTAR, M.; PETRU, J.; PAGAC, M.; KUTIOVA, K.; Complex View to Racing Car Upright Design and Manufacturing, *Manufacturing Technology 2018*, 18(3):449-456 DOI: 10.21062/ujep/120.2018/a/1213-2489/MT/18/3/449

[24] MINETOLA, P.; GALATI, M.; IULIANO, L.; ATZENI, E.; SALMI, A. Using self-replicated parts to improve the design and accuracy of an inexpensive 3D printer. *CIRP Procedure 2018*, 67, 203–208

[25] MINETOLA, P.; GALATI, M. The challenge of increasing the dimensional accuracy of a cheap 3D printer using self-replicable parts. *Add. Manuf. 2018*, 22, 256–264

[26] ISO. ISO 286-1:1988—ISO system of limits and fits. Part 1: Basis of tolerances, deviations and appropriateness; International Organization for Standardization (ISO): Gevena, Switzerland, 1988

[27] ISO. ISO 10360-2:2009 – Geometric specifications of a product (GPS) – Acceptance and verification tests for coordinate measuring instruments (CMM). Part 2: CMM used to measure linear dimensions; International Organization for Standardization (ISO): Gevena, Switzerland, 2009

[28] CONDRUZ, M.R.; PARASCHIV, A.; PUSCASU, C. Effect of heat treatment on hardness and microstructure of ADAM produced 17-4 PH. *Turbo 2018*, V, 39–45

[29] VIOLANTE, M.G.; IULIANO, L.; MINETOLA, P. Design and manufacture of fixtures for loose components using selective laser sintering. *Rapid prototype. J. 2007*, 13, 30–37